Hydroacoustic Signals Recorded by CTBTO Network Suggest a Possible Submarine Landslide in Trou Sans Fond Canyon, Offshore Ivory Coast, March 2024

Vaibhav Vijay Ingale*[1], Ross Parnell-Turner[1], Wenyuan Fan[1], Peter J. Talling[2], and Jeffrey Neasham[3]

Abstract

Underwater communication cables are essential components of global infrastructure, carrying over 99% of international data traffic. On 14 March 2024, a significant disruption to this network occurred because of a cable break offshore Ivory Coast, leading to widespread internet outages in the West African region. To investigate the cause of this cable break, we analyze hydroacoustic data recorded between 6 and 22 March on the two hydrophone triads installed near Ascension Island by the International Monitoring System of the Comprehensive Nuclear-Test-Ban Treaty Organization. We detect a low-frequency (< 60 Hz) signal on three northern and two southern triad hydrophones on 12 March 2024. The signal had a duration of 85 s on the north triad compared to 45 s on the south triad. We used the generalized cross correlation with phase transform method to show that the detected signal originated at a bearing of 38.9° ± 4.6°, consistent with the location of the cable break off Ivory Coast, and with steep bathymetric slopes mapped in the Trou Sans Fond Canyon. We do not observe associated signals on the nearby land-based seismic stations in Ghana and Ivory Coast, confirming the marine origin of this event. In addition, template matching shows that the same signal was not recorded in the preceding and following eight days, implying that this event was an isolated case. Given the scarcity of natural earthquakes offshore Ivory Coast, this combination of evidence suggests that the hydroacoustic signals are likely caused by a submarine landslide in the Trou Sans Fond Canyon. Our results show that an investigation of the causative submarine landslide events is also needed to realize the potential of these hydroacoustic methods for hazard risk assessment and mitigation.

Cite this article as Ingale, V. V., R. Parnell-Turner, W. Fan, P. J. Talling, and J. Neasham (2025). Hydroacoustic Signals Recorded by CTBTO Network Suggest a Possible Submarine Landslide in Trou Sans Fond Canyon, Offshore Ivory Coast, March 2024, *Seismol. Res. Lett.* **XX**, 1–11, doi: 10.1785/0220240448.

Supplemental Material

Introduction

Submarine landslides are gravitationally driven slope failures of the seabed that are commonly observed on submerged continental slopes, volcanic flanks, or within submarine canyons (Hampton *et al.*, 1996; Masson *et al.*, 2006; Chang *et al.*, 2021). Their size ranges from small, localized events to large, catastrophic collapses (Locat and Lee, 2002). Faster-moving landslides disintegrate and mix with surrounding seawater to create even more mobile seabed sediment flows called turbidity currents, which can travel for hundreds to thousands of kilometers into deep ocean basins (Piper *et al.*, 1999). Submarine landslides have the potential to trigger tsunamis, and together with associated turbidity currents they affect marine ecosystems, and cause damage to underwater infrastructure such as telecommunication cables and offshore installations (Harbitz *et al.*, 2006; Horrillo *et al.*, 2010; Talling *et al.*, 2022). However, it is extremely challenging to remotely sense and monitor submarine landslides in action. Indeed, we are yet to monitor a major submarine landslide in action in detail, anywhere in the global oceans (Talling *et al.*, 2014; 2023). This situation is a stark contrast to numerous direct observations of terrestrial landslides in action, and it ensures that submarine landslides are much more poorly understood (Locat and Lee, 2002; Masson *et al.*, 2006; Talling *et al.*,

1. Institute of Geophysics and Planetary Physics, Scripps Institution of Oceanography, University of California San Diego, La Jolla, California, U.S.A., https://orcid.org/0009-0009-2904-4764 (VVI); https://orcid.org/0000-0003-0641-3634 (RP-T); https://orcid.org/0000-0002-2983-8240 (WF); 2. Departments of Earth Science and Geography, Durham University, Durham, United Kingdom, https://orcid.org/0000-0001-5234-0398 (PJT); 3. Intelligent Sensing and Communications Group, School of Engineering, Newcastle University, Newcastle upon Tyne, United Kingdom, https://orcid.org/0000-0001-6059-9826 (JN)

*Corresponding author: vingale@ucsd.edu

2014). Here, we illustrate how hydroacoustic signals can potentially be used to remotely sense submarine landslides over large areas, using existing data collected by the International Monitoring System (IMS) of the Comprehensive Nuclear Test-Ban-Treaty Organization (CTBTO).

Instabilities leading to submarine landslides are caused by the imbalance between driving forces (e.g., gravitational force, earthquakes, and storm waves) and resisting strength, which can be weakened by factors such as pore water and gas pressures, groundwater seepage, or mass loading. When the driving force overcomes the resisting strength, the sediment mass collapses under gravity (Lee *et al.*, 2007). This collapse results in a rapid release of accumulated strain energy, which exerts pressure on the surrounding seafloor and triggers seismic waves that propagate through the Earth's crust (Masson *et al.*, 2006). In addition, the downslope movement can generate acoustic energy that propagates through the water column (Caplan-Auerbach *et al.*, 2001).

The only information from most submarine landslides comes from the scars and deposits they leave behind on the seabed, which are typically studied using techniques such as multibeam bathymetric mapping and side scan sonar imagery (e.g. in the southern Tyrrhenian Sea; Casas *et al.*, 2016), subsurface geophysical surveys (e.g., near Finneidfjord, Norway; Vardy *et al.*, 2012), and dated using geochronical and geochemical analysis (e.g., in the Gulf of Mexico; Dugan, 2012). These field data can be combined with numerical modeling to quantify slope instability (e.g., Puzrin *et al.*, 2016). Although these methods provide valuable insights into the characteristics of past events, they often fall short in capturing details about the initiation, duration, kinematics, and overall impact of submarine landslides (e.g., Clare *et al.*, 2024). Challenges in monitoring submarine landslides include logistical constraints related to long-term surveying at varying water depths (e.g., Clare *et al.*, 2017), their remote location (Urlaub and Villinger, 2019), and their unpredictable nature over time (Geist and Parsons, 2010). In addition, monitoring specific locations may overlook broader areas affected by instability (Gamboa *et al.*, 2021). Perhaps most importantly, the powerful nature of collapses can damage the monitoring infrastructure (e.g., Khripounoff *et al.*, 2012).

Underwater communication cables are essential infrastructure for global telecommunications (Carter *et al.*, 2009), yet are vulnerable to damage by submarine landslides (e.g., Pope *et al.*, 2017). Two particularly vulnerable areas are the Congo Canyon and Trou Sans Fond Canyon offshore West Africa. For example, turbidity currents in Congo Canyon have broken cables on six separate occasions between 2019 and 2024, highlighting the fragility of these critical communication links (Talling *et al.*, 2022; Baker *et al.*, 2024). Another notable incident occurred on 14 March 2024 at 04:46 UTC, when four cables serving West African countries suffered a break in the Trou Sans Fond Canyon (Booty and Garzeawu, 2024; Internet Society, 2024). These cable breaks occurred ∼107 km offshore from the city of Abidjan in the Ivory Coast, and in water depths of ∼3100 to 3300 m (Fig. 1a,b; personal communication). The resulting disruption on data traffic had a severe impact on internet speeds and communication across several West African countries, and it took several weeks to complete the necessary cable repairs (Internet Society, 2024; The Economist, 2024).

To investigate the origin of the cable breakages near the Ivory Coast in March 2024, we analyze hydroacoustic data from the IMS of the CTBTO, which maintains a global network of stations (Okal, 2001). This network has the potential for real-time monitoring and detection of underwater disturbances that could be associated with landslides. Hydrophones moored in the Sound Fixing and Ranging (SOFAR) channel record sound waves generated by geological events such as landslides, earthquakes, biological phenomena such as whale vocalization, and anthropogenic activities such as trawling and anchoring (e.g., Caplan-Auerbach *et al.*, 2001; Haver *et al.*, 2023; Romagosa *et al.*, 2020). For this study, we focused on hydroacoustic data recorded by hydrophones installed at the nearest CTBTO station, HA10 near Ascension Island, ∼1811 km from the Le Trou Sans Fond Canyon (Fig. 1a,c).

Data

The HA10 Ascension IMS station consists of two triads of hydrophones moored within the SOFAR channel to the north and south of Ascension Island (H10N and H10S, respectively), arranged in a triangular configuration with a spacing of ∼2 km between each receiver (Fig. 1c). These hydrophones continuously record acoustic waves at a sampling rate of 250 Hz with 24-bit analog-to-digital resolution (Table 1). For this analysis, we examined acoustic data from both triads between 8 and 22 March 2024. Because of a poor signal-to-noise ratio during this time period, data from the hydrophone at H10S1 within the H10S triad were excluded from the analysis.

Results

Signal characteristics

We conducted an initial visual inspection of hydroacoustic data from the H10N and H10S triads, identifying seven candidate signals recorded between 6 and 22 March based on their frequency content, duration, and spectral energy differences between the two triads. To further assess these signals, we calculated their first arrivals at the north and south triads. This analysis allowed us to eliminate signals that arrived at the south triad prior to the north triad (e.g., on 9 March at 13:20 UTC and 13 March at 14:05 UTC; Figs. S1 and S2, available in the supplemental material to this article) because events originating from the Trou Sans Fond Canyon would arrive on the north triad first. Out of remaining candidates, a signal on 13 March at 01:47 UTC was observed only on H10S2 and H10S3 of the south triad, with no corresponding detection on the north triad (Fig. S3).

On 12 March 2024, two days before the reported offshore cable break near the Ivory Coast (Fig. 1), a signal was recorded

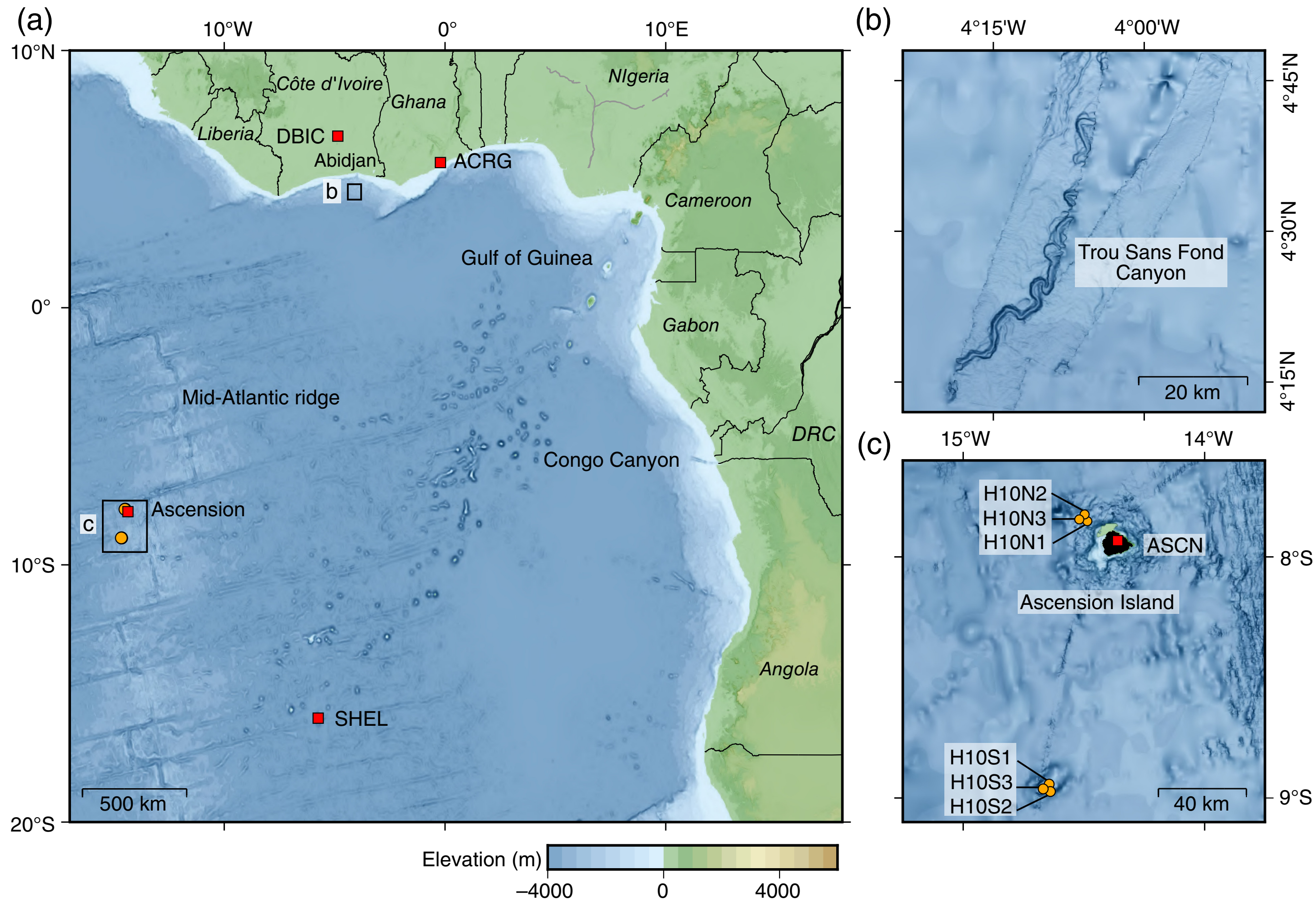

arriving at the north triad prior to its arrival at the south triad (Fig. 2). Within the north triad, the signal was initially recorded by the hydrophone at H10N2 at 08:31:21 UTC, followed by H10N1, and then H10N3. In the south triad, the signal was first recorded by H10S2 at 08:32:32 UTC, followed by H10S3. There is neither a report of this signal in the bulletin of reviewed events of the International Data Center of CTBTO, nor are these events in the International Seismological Centre catalog. The signal lasted for ~85 s on the north triad, with frequencies reaching up to 60 Hz, and ~45 s on the south triad, with frequencies up to 20 Hz. The waveform on the north triad displayed higher amplitude compared to that on the south

Figure 1. (a) Regional map of West Africa region: regions near Ivory Coast and Ascension Island are extended in panels (b) and (c). Red squares mark location of land-based seismometers and orange circles show hydrophone triads near Ascension Island. (b) Bathymetry of Trou Sans Fond Canyon (Ryan *et al.*, 2009) along which cable break incident reported. (c) North (H10N) and south (H10S) triads of three hydrophones deployed by the International Monitoring System Comprehensive Nuclear Test-Ban-Treaty Organization (IMS-CTBTO) near Ascension Island. The color version of this figure is available only in the electronic edition.

TABLE 1
Location Parameters of the Hydrophones at Station HA10, near Ascension Island, Atlantic Ocean

Site	H10N1	H10N2	H10N3	H10S1	H10S2	H10S3
Latitude (°S)	7.8456	7.8278	7.8409	8.9412	8.9591	8.9527
Longitude (°W)	14.4802	14.4875	14.5017	14.6484	14.6453	14.6629
Depth below sea surface (m)	800	800	800	800	800	800
Sampling rate (Hz)	250	250	250	250	250	250

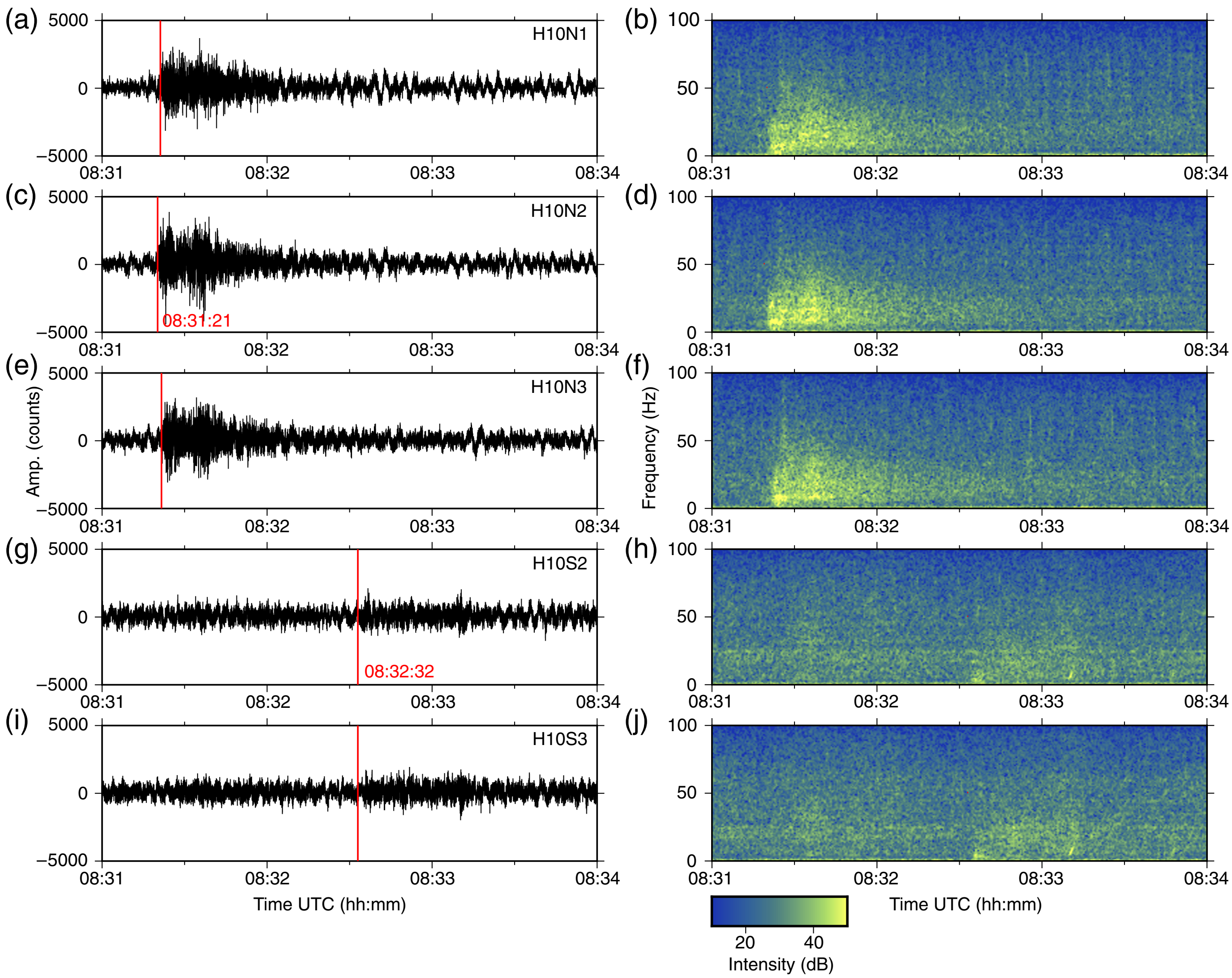

Figure 2. (a,c,e,g,i) Waveforms and (b,d,f,h,j) spectrograms from three hydrophones of north (H10N1, H102, and H10N3) and two of south (H10S2 and H10S3) triads on 12 March 2024. Red lines mark signal arrival with times noted; first arrival from each triad is marked on H10N2 and H10S2. The color version of this figure is available only in the electronic edition.

triad, likely due to the obstruction of acoustic waves by the bathymetric slopes around Ascension Island. The time difference between the arrival times at the two triads was 71 s. We calculated water velocity using average temperature and salinity data obtained from a hindcast of the World Ocean Atlas (Reagan *et al.*, 2024) along a great circle path between north triad and the Trou Sans Fond Canyon, sampled at 25 km intervals at a SOFAR channel depth of 800 m (Fig. S4). The resulting average water velocity within the SOFAR channel was 1.482 km/s. Multiplying by the time difference (71 s), we obtain a source–receiver distance of ~105 km, which is consistent with intertriad spacing of 107 km.

Direction of signal arrival

Although we cannot precisely pinpoint the exact source location of these signals with the available data, we can estimate the directionality of the arriving acoustic signals by analyzing the time lag or time difference of arrival (TDOA) across three hydrophones of the north triad. We employed the generalized cross-correlation with phase transform (GCC-PHAT) method, for which we first calculated the cross-power spectrum between 85-s-long signals (filtered between 1 and 60 Hz) from two hydrophones using the fast Fourier transform (FFT). We then applied a phase transform weighting through amplitude normalization, followed by an inverse FFT to derive the TDOA (e.g., Johnson and Dudgeon, 1993). A positive TDOA indicates that the signal arrived at the first hydrophone later than at the second, whereas a negative time lag suggests the opposite.

The resulting correlation coefficient (CC) exhibited multiple peaks at different time lags (Fig. 3a). To isolate distinct time lag values for each hydrophone pair, we applied a threshold based on the median absolute deviation of the CC, which is the median of the absolute differences between each CC

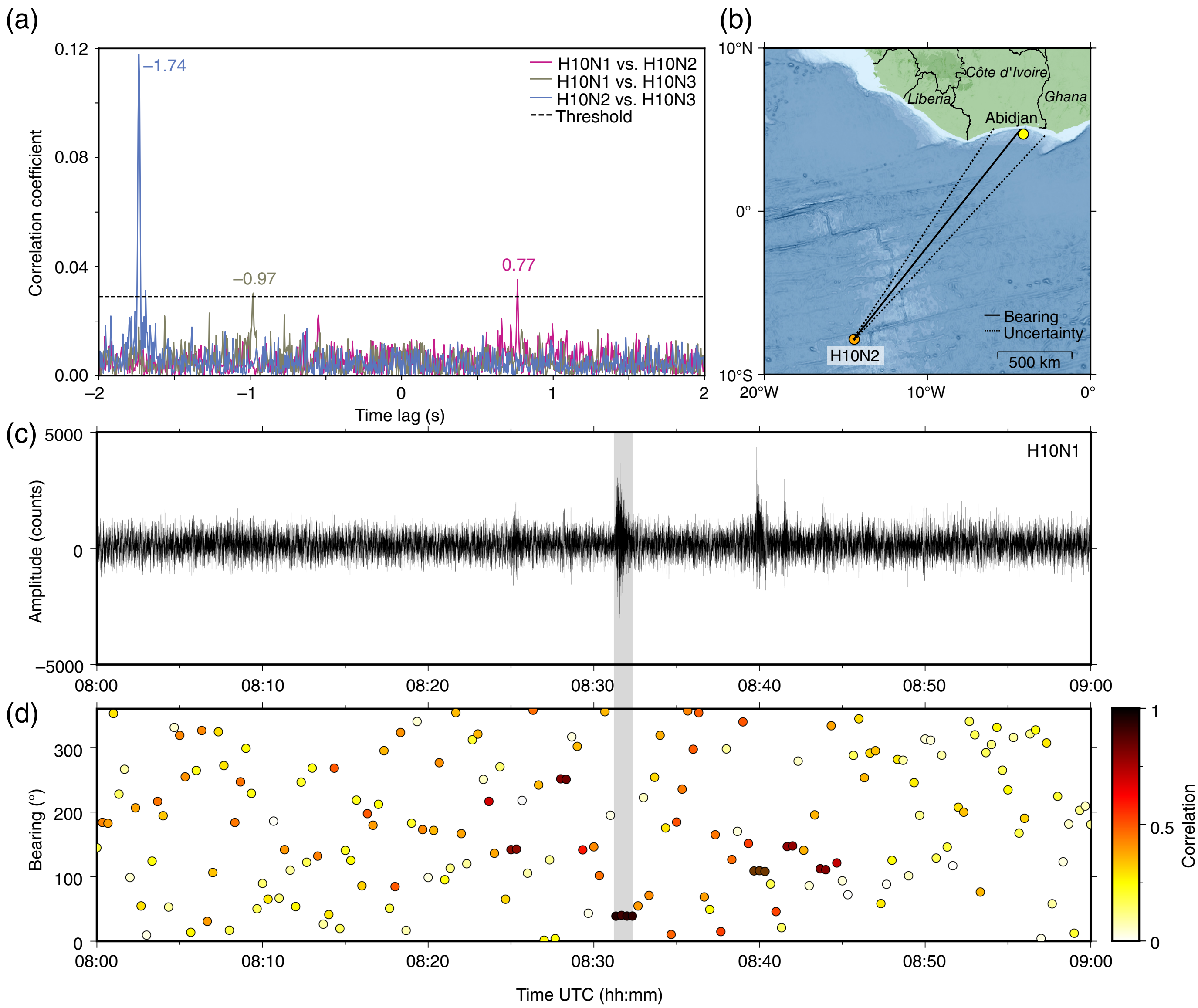

Figure 3. (a) Generalized cross-correlation with phase transform (GCC-PHAT) for each pair of hydrophones of the north triad, H10N1 and H10N2, H10N1 and H10N3, and H10N2 and H10N3. Threshold (dashed line) is defined as average of median absolute deviation of correlation coefficient (CC) for three pairs. (b) Bearing of signal (solid line) computed from time lags of cross correlation and associated uncertainties (dashed lines). Yellow circle marks the Trou Sans Fond Canyon. (c) One-hour-long waveform of a signal on H10N1. (d) Temporal distribution of bearing for a signal shown in panel (c), shaded by CC. Gray-colored region shows coincidence of signal with bearing at ~39° and having high-correlation values. The color version of this figure is available only in the electronic edition.

and the median of the CC. We identified three distinct peaks for each hydrophone pair above the threshold, with the signal arriving at H10N2 first, followed by H10N1 with a delay of 0.77 s, and finally at H10N3 with a delay of 1.74 s (Fig. 3a). The TDOA between H10N1 and H10N3 was 0.97 s.

We converted the TDOA values into distance differences after multiplying by the water velocity of 1.482 km/s. Using the hydrophone locations and the calculated distance differences, we formulated an objective function in the form of a hyperbolic equation:

$$f(x,y) = \sum_{i,j=1}^{3} \left(\sqrt{(x - x_i)^2 + (y - y_i)^2} - \sqrt{(x - x_j)^2 + (y - y_j)^2} - \Delta d_{ij} \right)^2,$$

in which i, j are hydrophone numbers; (x_1, y_1), (x_2, y_2), (x_3, y_3) are coordinates of hydrophones at H10N1, H10N2, and H10N3, respectively; Δd_{ij} is the distance difference between each pair of hydrophones i, j obtained by multiplying TDOA by water velocity. By minimizing this objective function for each pair of hydrophones, we identified a common intersection point of the hyperbolic equations and determined a bearing of

TABLE 2

Estimated Arrival Time of Signal on Four Land-Based Seismometers in Global Seismic Network (GSN) Around Ivory Coast (Locations Shown in Fig. 1a)

GSN Stations	DBIC	ACRG	ASCN	SHEL
Location	Ivory Coast	Ghana	Ascension Island	Saint Helena Island
Latitude	6.6701° N	5.6415° N	7.9327° S	15.9594° S
Longitude	4.8565° W	0.2011° W	14.3601° W	5.7455° W
Distance from cable break (km)	230	444	1811	2306
Rayleigh-wave velocity (km/s)	3.25	3.25	–	–
Water velocity (km/s)	–	–	1.482	1.482
Estimated arrival time (UTC)	08:12:11	08:13:17	08:31:22	08:36:57

38.9°, calculated as the angle between the line from one hydrophone to the intersection point (Fig. 3b). To evaluate uncertainty in this bearing estimate, we computed water velocities along the great circle path between the north triad and the cable break location at 50 m intervals for depths between 600 and 1000 m (±200 m around the nominal SOFAR channel depth of 800 m). The bearing uncertainties were derived from the objective function minimization for each depth interval, and obtained a value of ±4.6°.

We also computed the temporal distribution of bearing over an hour-long waveform from 08:00 UTC to 09:00 UTC (Fig. 3c), at 20 s intervals (e.g., Gibbons, 2022). We first computed pairwise correlations for each hydrophone pair, H10N1 versus H10N2, H10N1 versus H10N3, and H10N2 versus H10N3. The resulting pairwise CCs were averaged and normalized to derive a multistation correlation metric, which provides a more robust estimate of signal coherence (Fig. 3c). For each 20 s interval, the corresponding correlation time lags were determined and inverted to estimate the bearing of the signal relative to the north triad. We observed high-correlation values (>0.8) at six different instances between 08:28 and 08:45 UTC (Fig. 3d). Out of them only a signal between 08:31:20 and 08:32:00 UTC showed a bearing 38.9° ± 4.6° representing the most probable direction of arrival for the waveform over the signal's duration. Remaining five instances (signals) showed bearings in southeast and northwest directions.

The projected signal bearing computed in two ways is consistent (~39°) from the H10N triad and aligns with the Trou Sans Fond Canyon (Fig. 3b,d). It is a sinuous canyon feature that originates at the coast, and extends >100 km offshore (e.g., Martin, 1970; Dietz and Knebel, 1971). Bathymetric mapping of the canyon in the region of the cable crossing was completed in 2021 on M/V Fugro Supporter, using an EM122 echosounder yielding a ~60 m resolution grid (Ryan *et al.*, 2009). These data show that the canyon near the computed bearing location is >300 m deep and ~1 km wide, with slopes typically ranging from 25° to 35° (refer to the Discussion section), which could be susceptible to mass-wasting and failure leading to submarine landslides.

For three remaining signals from seven candidate signals (9 March at 16:42, 11 March at 16:56, and 14 March 04:47 UTC), the corresponding bearings were mostly north-northwest with values 330.5° ± 3.5°, 327.7° ± 3.4° and 312.5° ± 2.8°, respectively (Figs. S5–S7). This result eliminates their association with cable break near Trou Sans Fond Canyon and confirms that a signal at 08:31 UTC on 12 March is linked to the cable break incidence.

Discussion

Absence of signal on land-based seismometers

Although the acoustic signal directionality aligns with the cable break location, we wish to eliminate the likelihood of a terrestrial, rather than underwater origin of the detected signal. We obtained three-component (E, N, and Z) data from four land-based seismometer stations in the Global Seismic Network (GSN) located west of Africa and within the uncertainty of bearing estimate (Table 2). Given the cable break occurred in Trou San Fond Canyon and is ~1809 km from the north triad, we estimated the origin time of the signal to be 08:11:01 UTC on 12 March 2024, assuming the uniform water velocity of 1.482 km/s between source and hydrophone triad. Using this origin time and the distances of the land-based seismometer locations from the canyon, we calculated the expected arrival times of this signal at each of the four seismometers (Table 2). The calculations take into account the propagation of Rayleigh surface waves with a group velocity of 3.25 km/s for upper continental crust (Stein and Wysession, 2009; Shearer, 2019) up to Dimborko Cote d'Ivoire (DBIC) and Accra Ghana (ACRG) seismometers, deployed in Ivory Coast and Ghana, respectively, assuming that the acoustic waves converted to surface waves at the shoreline. We disregarded the acoustic travel time between the source location and coastline. For Ascension (ASCN) and Horse Pasture, Island of Saint Helena (SHEL) stations deployed on Ascension and Saint Helena Islands, respectively, we consider the acoustic travel time along the solid Earth path to be insignificant compared to the acoustic path. Upon reviewing the seismic records (Figs. S8–S11), we did not find any signals that matched the expected arrival times. This absence of corresponding signals supports the marine origin for the detected signal, likely associated with a submarine landslide in Trou Sans Fond Canyon leading to seabed cable break. To our knowledge, this is the first study demonstrating a submarine landslide signal detected by hydrophones, apart from landslides caused by volcanic eruptions (e.g., Caplan-Auerbach *et al.*, 2001, 2014; Wright *et al.*, 2008; Chadwick *et al.*, 2012; Tepp and Dziak, 2021) or by strong earthquakes (Okal, 2003).

Template-matching detection

We evaluated whether the observed acoustic signal was an isolated event or part of a recurring pattern using a template-matching detection approach. Our aim is to establish whether similar signals were present at other times, which could imply a different source or mechanism to that of an isolated submarine landslide event. First, we extracted a 20-s-long waveform template starting from the signal's arrival time on each hydrophone of both the north and south triads. Although the duration of signal was different on either of the triads (85 s on north and 45 s on south triad), to minimize the influence of noise and to handle any presence of overlapping signals, we selected a signal for 20 s long duration. Next, we computed CCs with the continuous waveforms recorded between 6 and 22 March 2024, filtered between 1 and 60 Hz. Example day-long waveforms recorded on the H10N1 hydrophone between 10 and 14 March, and the corresponding CCs, are shown in Figure 4. The template-matching results for the other four hydrophones (H10N2, H10N3, H10S2, and H10S3) are shown in Figures S12–S15.

To identify detections similar to the observed signal, a threshold of eight times the median absolute deviation of the CC was established. When the threshold was set at seven times the median absolute deviation, it led to all CCs for certain stations on specific dates (e.g., H10N2 on 10–12 March and H10S3 on 12 March) exceeding the threshold, resulting in false positive detections. Therefore, a multiplier of eight was chosen to prevent such false positives. We observed a detection on H10N3 above the threshold at 07:29 UTC on 10 March (Fig. S12), but no corresponding detection was observed on the other hydrophones. Apart from the self-detection (Fig. 4c), no similar signals were observed throughout the 16-day period, suggesting that the signal on 12 March was an isolated event, and not part of a repeating pattern.

On 14 January 2020, a series of cable breaks occurred in Congo Canyon, caused by a long runout (>1000 km) turbidity current (Talling *et al.*, 2022; Baker *et al.*, 2024). To determine whether a similar acoustic signal was observed near Trou Sans Fond Canyon on 12 March 2024, we performed template matching on continuous hydrophone data collected between 10 and 14 January 2020, using 08:31 UTC signal. However, we did not find any instances of template matches that could be associated with the Congo Canyon cable-breaking event (Figs. S16, S17). This may suggest the Congo Canyon turbidity current was initiated by a smaller-volume or slower-moving landslide, or other processes such as fluid-mud layers formed at spring tides in the Congo River's estuary (see Talling *et al.*, 2022 for a full discussion).

The observed signal, with a frequency reaching up to 60 Hz and detected only once, is inconsistent with common anthropogenic sources, which generally operate at higher frequencies and are repetitive in nature. For example, seismic air gun shots typically generate low-frequency signals between 10 and 200 Hz, but they are characterized by regular, repeated signals over extended periods (Estabrook *et al.*, 2016). Similarly, shipping noise excites energies at frequencies between 20 and 400 Hz, and this noise is persistent over long time periods (i.e., hours to days; Niu *et al.*, 2017). Other anthropogenic sources, such as active sonar experiments operate at midfrequency (1–2 kHz) and high frequency (2–10 kHz) and are unlikely to cause the observed signal. Offshore construction activities such as piling installation and operations associated with offshore hydrocarbon platforms concentrate their energy in the 100 Hz to 2 kHz (Miksis-Olds *et al.*, 2013). Given that none of these sources match the observed signal's frequency or singular occurrence, it is unlikely to be associated with anthropogenic activities.

The short-duration (~45 to 85 s) of this signal is probably due to a sudden and localized nature of the initial landslide. This landslide may involve rapid destabilization of sediment from a steep slope along canyon wall that could possibly create acoustics signals as the material interacts with the seafloor or water column. The landslide may then have disintegrated and mixed with surrounding seawater to form a much longer duration (and runout distance) turbidity current, but which did not produce a hydroacoustic signal.

Time lag between signal and cable break incident

The cable break incident occurred at 04:46 UTC on 14 March 2024, following a signal that originated at 08:11 UTC on 12 March, resulting in a total elapsed time of 160,500 s. The great circle (i.e., direct) distance from the cable break site to the mouth of the submarine canyon near the Abidjan coast is approximately 101 km, whereas the distance following the sinuous submarine canyon axis is ~115 km (Fig. 5a). Assuming that a slope failure initiated in the high-slope region near the coast and triggered a mass-transport flow, which took 160,500 s to traverse this distance, we obtain an average speed of 0.72 m/s, reflecting the uncertainty in path length (Fig. 5b). This speed is significantly lower than the range of front speeds for landslide-triggered sediment flows that break seabed cables (1.8–20 m/s; table 1 of Talling *et al.*, 2013, 2022; Carter *et al.*, 2014; Pope *et al.*, 2017).

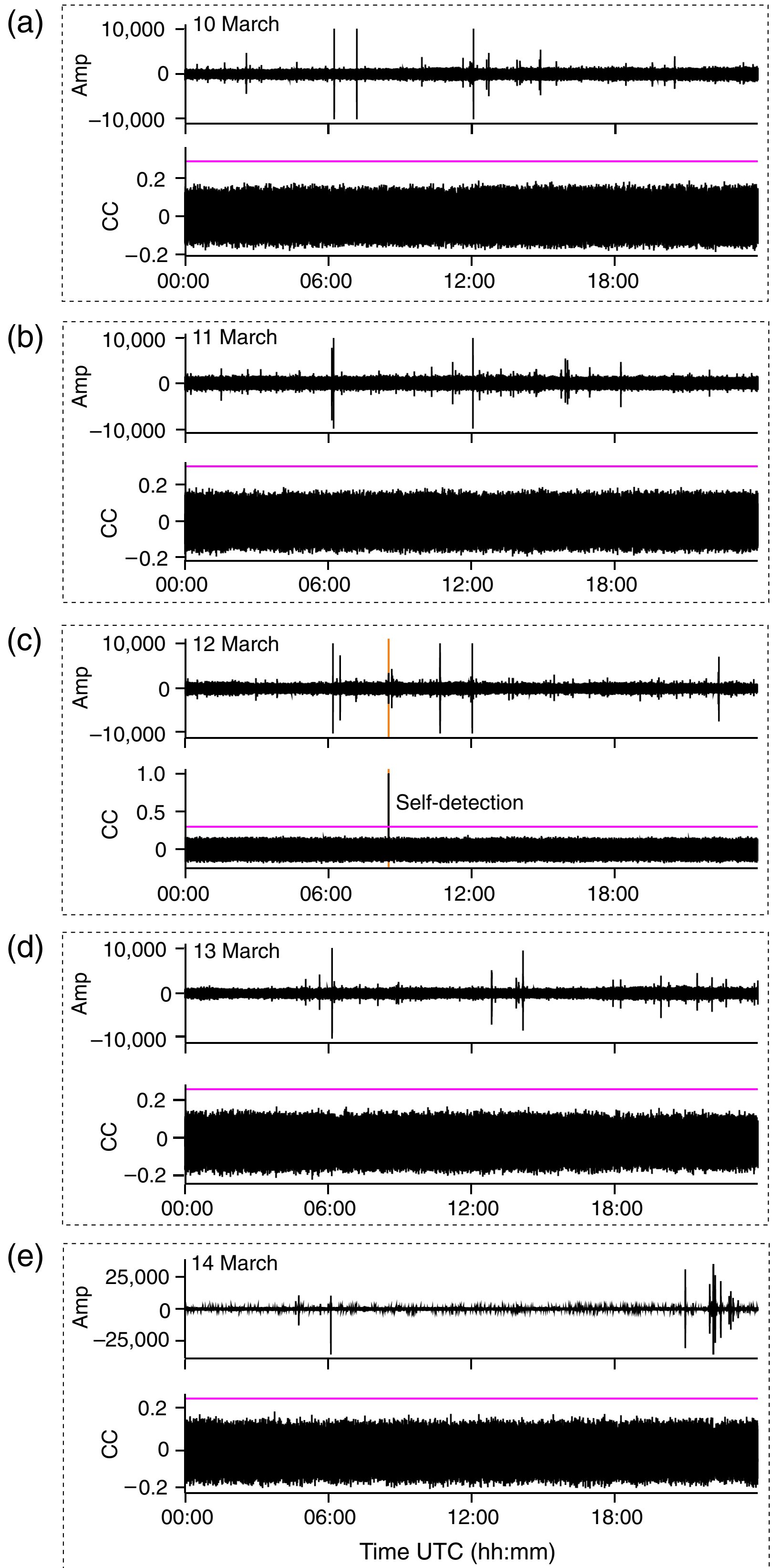

Figure 4. Template matching between a 20 s signal (Fig. 2) and day-long continuous data from H10N1 hydrophone in 2024. Upper panels show waveform and lower panels show CC for (a) 10, (b) 11, (c) 12, (d) 13, and (e) 14 March. Magenta line indicates detection threshold, with detections exceeding threshold highlighted in orange (e.g., self-detection on 12 March). The color version of this figure is available only in the electronic edition.

Although a front speed of 0.72 m/s is not implausible for sediment flows that can result in cable breaks, it is important that this average front speed may not represent the maximum speed reached during the flow (e.g., Talling *et al.*, 2022). Sediment flows often exhibit complex behaviors characterized by varying front velocities over time and distance. The initial triggering event, such as a submarine slope failure, could cause a turbidity current that progressively accelerated along the canyon. Such changes in flow speed may result from incorporation of sediment from the seabed, causing the turbidity current to become denser and thus faster (Parker *et al.*, 1986; Talling *et al.*, 2023). Flow acceleration may lead to significantly higher speeds at the site of the cable break than the average calculated from the flow's source location to the cable break (Covault, 2011; Talling *et al.*, 2023). Thus, it is possible that a turbidity current traveling along the Trou Sans Fond Canyon with an average speed of 0.72 m/s from its near-coast landslide source, had significantly higher speeds at the site of the offshore cable break.

Conclusions

Using real-time hydroacoustic data recorded near Ascension Island by IMS-CTBTO hydrophones, we identified a low-frequency acoustic signal at 08:11 on 12 March 2024. The signal's direction broadly aligns with the site of a submarine cable break at 04:46 on 14 March 2024 in the Trou Sans Fond Canyon, ~100 km offshore Ivory Coast. This cable

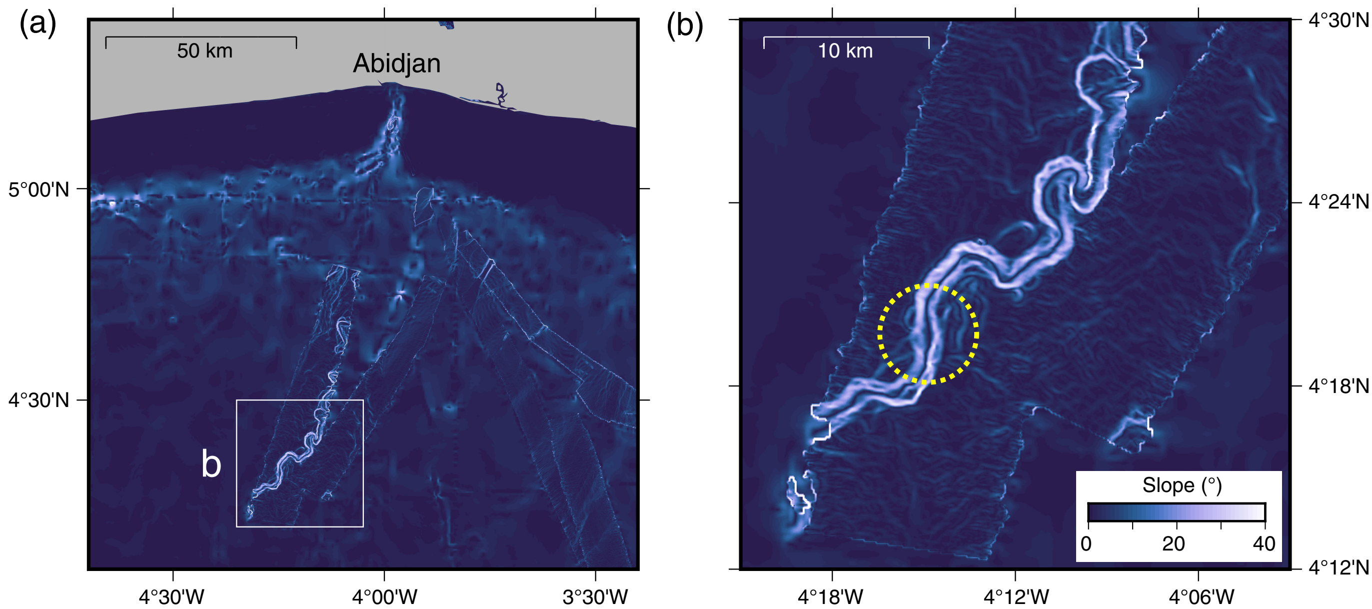

Figure 5. (a) Slope map derived from bathymetry data (Ryan *et al.*, 2009), highlighting steeper gradients at canyon mouth near Abidjan and extending further south. (b) Detailed view of the Trou Sans Fond Canyon showing slope variations along sinusoidal path. Yellow circle indicates the approximate location of cable break (personal communication). The color version of this figure is available only in the electronic edition.

break was due to a seabed turbidity current that occurred ~44 hr after the low-frequency signal, and which also broke a series of cables further down the Trou Sans Fond Canyon. The turbidity current was likely triggered by a submarine landslide in the steeper upper part of the Trou Sans Fond Canyon, closer to the coast. This delay of ~44 hr is thus consistent with the time needed for a landslide-derived turbidity current to travel ~115 km down the Trou Sans Canyon at an average speed of ~0.72 m/s. An examination of waveforms from land-based seismometers in the West African region confirms that the signal is not terrestrial in origin, consistent with a marine signal origin. To definitively confirm a causative mechanism, additional seafloor data are needed, such as multibeam or side-scan sonar mapping that identifies the location of this recent landslide scar. However, this study shows for the first time how integrating real-time capabilities of the CTBTO network with such seafloor mapping could significantly enhance monitoring and understanding of submarine geohazards in future. This detection can be achieved based on spectral analysis of different types of signals, their direction of arrival, their uniqueness and time lag between signal detection and an event.

Data and Resources

The hydroacoustic data analyzed in this study are available on Incorporated Research Institutions of Seismology (IRIS, https://service.iris.edu/fdsnws/dataselect/docs/1/builder/, last accessed July 2024) database. Bathymetric data in Figures 1b,c and 3b were obtained from the Global Multi-Resolution Topography compilation (Ryan *et al.*, 2009). Figures made with the Generic Mapping Tools (GMT, Wessel *et al.*, 2019); template matching was performed using ObsPy (Beyreuther *et al.*, 2010); temperature and salinity data to compute the water velocity were obtained from World Ocean Atlas (Reagan *et al.*, 2024). The supplemental material contains waveforms and spectrograms of six candidate signals between 9 and 14 March, of four land-based seismometers recorded between 07:55 and 08:40 UTC on 12 March 2024, template-matching results for H10N1, H10N3, H10S2, and H10S3 stations between 10 and 14 March and for H10N1 and H10NS2 stations between 10 and 14 January 2020.

Declaration of Competing Interests

The authors acknowledge that there are no conflicts of interest recorded.

Acknowledgments

This work is supported by the Institute of Geophysics and Planetary Physics' Green Foundation Fellowship. The authors thank two anonymous reviewers who provided helpful feedback.

References

Baker, M. L., P. J. Talling, R. Burnett, E. L. Pope, S. C. Ruffell, M. Urlaub, M. A. Clare, J. Jenkins, M. Dietze, J. Neasham, *et al.* (2024). Seabed seismographs reveal duration and structure of longest runout sediment flows on earth, *Geophys. Res. Lett.* **51,** no. 23, e2024GL111078, doi: 10.1029/2024GL111078.

Beyreuther, M., R. Barsch, L. Krischer, T. Megies, Y. Behr, and J. Wassermann (2010). ObsPy: A python toolbox for seismology, *Seismol. Res. Lett.* **81,** no. 3, 530–533, doi: 10.1785/gssrl.81.3.530.

Booty, N., and M. K. Garzeawu (2024). South Africa, Nigeria, Ghana, Liberia and Ivory Coast hit by major internet outages, *BBC News*, available at https://www.bbc.com/news/world-africa-68569022 (last accessed July 2024).

Caplan-Auerbach, J., R. P. Dziak, D. R. Bohnenstiehl, W. W. Chadwick, and T.-K. Lau (2014). Hydroacoustic investigation of submarine landslides at West Mata volcano, Lau Basin, *Geophys. Res. Lett.* **41,** no. 16, 5927–5934, doi: 10.1002/2014GL060964.

Caplan-Auerbach, J., C. G. Fox, and F. K. Duennebier (2001). Hydroacoustic detection of submarine landslides on Kilauea volcano, *Geophys. Res. Lett.* **28,** no. 9, 1811–1813, doi: 10.1029/2000GL012545.

Carter, L., D. Burnett, S. Drew, G. Marle, L. Hagadorn, D. Bartlett-McNeil, and N. Irvine (2009). Submarine cables and the Oceans – connecting the world, *UNEP-WCMC Biodiversity Series No. 31. ICPC/UNEP/UNEP-WCMC.*

Carter, L., R. Gavey, P. J. Talling, and J. T. Liu. (2014). Insights into submarine geohazards from breaks in subsea telecommunication cables, *Oceanography* **27,** no. 2, 58–67, doi: 10.5670/oceanog.2014.40.

Casas, D., F. Chiocci, D. Casalbore, G. Ercilla, and J. O. De Urbina (2016). Magnitude-frequency distribution of submarine landslides in the Gioia Basin (southern Tyrrhenian Sea), *Geo-Mar. Lett.* **36,** no. 6, 405–414, doi: 10.1007/s00367-016-0458-2.

Chadwick, W. W., R. P. Dziak, J. H. Haxel, R. W. Embley, and H. Matsumoto (2012). Submarine landslide triggered by volcanic eruption recorded by in situ hydrophone, *Geology* **40,** no. 1, 51–54, doi: 10.1130/G32495.1.

Chang, Y.-C., N. C. Mitchell, and R. Quartau (2021). Landslides in the upper submarine slopes of volcanic islands: The central Azores, *Geochem. Geophys. Geosys.* **22,** e2021GC009833, doi: 10.1029/2021GC009833.

Clare, M. A., G. Lintern, E. Pope, M. Baker, S. Ruffell, M. Z. Zulkifli, S. Simmons, M. Urlaub, M. Belal, and P. J. Talling (2024). *Seismic and Acoustic Monitoring of Submarine Landslides*, in *Noisy Oceans*, G. Bayrakci and F. Klingelhoefer (Editors), AGU Geophysical Monograph Series, doi: 10.1002/9781119750925.ch5.

Clare, M. A., M. E. Vardy, M. J. B. Cartigny, P. J. Talling, M. D. Himsworth, J. K. Dix, J. M. Harris, R. J. S. Whitehouse, and M. Belal (2017). Direct monitoring of active geohazards: emerging geophysical tools for deep-water assessments, *Near Surf. Geophys.* **15,** 427–444, doi: 10.3997/1873-0604.2017033.

Covault, J. A. (2011). Submarine fans and canyon-channel systems: A review of processes, products, and models, *Nat. Educ. Knowl.* **3,** no. 10, 4.

Dietz, R. S., and H. J. Knebel (1971). Trou sans fond submarine canyon: Ivory Coast, Africa, *Deep Sea Res. Oceanogr. Abstr.* **18,** no. 4, 441–447, doi: 10.1016/0011-7471(71)90105-7.

Dugan, B. E. (2012). Petrophysical and consolidation behavior of mass transport deposits from the northern Gulf of Mexico, IODP Expedition 308, *Mar. Geol.* **315,** 98–107, doi: 10.1016/j.margeo.2012.05.001.

Estabrook, B. J., D. W. Ponirakis, C. W. Clark, and A. N. Rice (2016). Widespread spatial and temporal extent of anthropogenic noise across the northeastern Gulf of Mexico shelf ecosystem, *Endanger. Species Res.* **30,** 267–282, doi: 10.3354/esr00743.

Gamboa, D., R. Omira, and P. Terrinha (2021). A database of submarine landslides offshore West and Southwest Iberia, *Sci. Data* **8,** 185, doi: 10.1038/s41597-021-00969-w.

Geist, E. L., and T. Parsons (2010). Estimating the empirical probability of submarine landslide occurrence, in *Submarine Mass Movements and their Consequences*, D. C. Mosher, *et al.* (Editors), 377–386, Springer, Dordrecht, Netherlands, doi: 10.1007/978-90-481-3071-9_31.

Gibbons, S. J. (2022). The hydroacoustic network of the CTBT international monitoring system: Access and exploitation, *J. Peace Nuclear Disarmament* **5,** no. 2, 452–468, doi: 10.1080/25751654.2022.2129948.

Hampton, M. A., H. J. Lee, and J. Locat (1996). Submarine landslides, *Rev. Geophys.* **34,** no. 1, 33–59, doi: 10.1029/95RG03287.

Harbitz, C. B., F. Løvholt, G. Pedersen, and D. G. Masson (2006). Mechanisms of tsunami generation by submarine landslides: a short review, *Norw. J. Geol.* **86,** no. 3, 255–264.

Haver, S. M., J. Haxel, R. P. Dziak, L. Roche, H. Matsumoto, C. Hvidsten, and L. G. Torres (2023). The variable influence of anthropogenic noise on summer season coastal underwater soundscapes near a port and marine reserve, *Mar. Pollut. Bull.* **194,** 115406, doi: 10.1016/j.marpolbul.2023.115406.

Horrillo, J., A. Wood, C. Williams, A. Parambath, and G. Kim (2010). Construction of Tsunami Inundation Maps in the Gulf of Mexico, *Report Award Number: NA09NWS4670006*, National Tsunami Hazard Mitigation Program (NTHMP), National Weather Service Program Office, NOAA.

Internet Society (2024). 2024 West Africa submarine cable outage report, available at https://www.internetsociety.org/wp-content/uploads/2024/04/2024-West-Africa-Submarine-Cable-Outage-Report.pdf (last accessed July 2024).

Johnson, D. H., and D. E. Dudgeon (1993). *Array Signal Processing: Concepts and Techniques*, Prentice Hall Signal Processing Series, PTR Prentice Hall, New Jersy, USA.

Khripounoff, A., C. Philippe, N. Lo Bue, D. Bernard, and S. J. Ricardo (2012). Different types of sediment gravity flows detected in the Var submarine canyon (northwestern Mediterranean Sea), *Prog. Oceanogr.* **106,** 138–153, doi: 10.1016/j.pocean.2012.09.001.

Lee, H. J., J. Locat, P. Desgagnés, J. D. Parsons, B. G. McAdoo, D. L. Orange, P. Puig, F. L. Wong, P. Dartnell, and E. Boulanger (2007). Submarine mass movements on continental margins, in *Continental Margin Sedimentation*, I. Jarvis, C. A. Nittrouer, J. A. Austin, M. E. Field, J. H. Kravitz, J. P. M. Syvitski, and P. L. Wiberg (Editors), Blackwell Publishing, Oxford, UK, doi: 10.1002/9781444304398.ch5.

Locat, J., and H. J. Lee (2002). Submarine landslides: Advances and challenges, *Can. Geotech. J.* **39,** no. 1, 193–212, doi: 10.1139/t01-089.

Martin, L. (1970). Premières investigations sur l'origine du Trou-Sans-Fond, canyon sous-Marin de la Côte d'Ivoire, *C. R. Acad. Sci.* **270,** no. 1, 32–35 (in French).

Masson, D. G., C. B. Harbitz, R. B. Wynn, G. Pedersen, and F. Løvholt (2006). Submarine landslides: processes, triggers and hazard prediction, *Phil. Trans. Roy. Soc. Lond. A* **364,** no. 1845, 2009–2039, doi: 10.1098/rsta.2006.1810.

Miksis-Olds, J. L., D. L. Bradley, and X. NiuMaggie (2013). Decadal trends in Indian Ocean ambient sound, *J. Acoust. Soc. Am.* **134,** no. 5, 3464–3475, doi: 10.1121/1.4821537.

Niu, H., E. Ozanich, and P. Gerstoft (2017). Ship localization in Santa Barbara Channel using machine learning classifiers, *J. Acoust. Soc. Am.* **142,** no. 5, EL455–EL460, doi: 10.1121/1.5010064.

Okal, E. A. (2001). T-phase stations for the international monitoring system of the comprehensive nuclear-test ban treaty: A global perspective, *Seismol. Res. Lett.* **72,** no. 2, 186–196, doi: 10.1785/gssrl.72.2.186.

Okal, E. A. (2003). *T* waves from the 1998 Papua new guinea earthquake and its aftershocks: Timing the tsunamigenic slump, in *Landslide Tsunamis: Recent Findings and Research Directions*, J. P. Bardet, F. Imamura, C. E. Synolakis, E. A. Okal, and H. L. Davies (Editors), Pageoph Topical Volumes, Birkhäuser, Basel, Switzerland, doi: 10.1007/978-3-0348-7995-8_4.

Parker, G., Y. Fukushima, and H. M. Pantin (1986). Self-accelerating turbidity currents, *J. Fluid Mech.* **171,** 145–181.

Piper, D. J., P. Cochonat, and M. L. Morrison (1999). The sequence of events around the epicentre of the 1929 Grand Banks earthquake: initiation of debris flows and turbidity current inferred from side scan sonar, *Sedimentology* **46,** no. 1,79–97, doi: 10.1046/j.1365-3091.1999.00204.x.

Pope, E. L., P. J. Talling, and L. Carter (2017). Which earthquakes trigger damaging submarine mass movements: Insights from a global record of submarine cable breaks? *Mar. Geol.* **384,** 131–146, doi: 10.1016/j.margeo.2016.01.009.

Puzrin, A. M., L. N. Germanovich, and B. Friedli (2016). Shearband propagation analysis of submarine slope stability, *Géotechnique* **66,** no. 3, 188–201, doi: 10.1680/jgeot.15.LM.002.

Reagan, J. R., T. P. Boyer, H. E. García, R. A. Locarnini, O. K. Baranova, C. Bouchard, S. L. Cross, A. V. Mishonov, C. R. Paver, D. Seidov, *et al.* (2024). World Ocean Atlas 2023, *NOAA National Centers for Environmental Information*, Dataset: NCEI Accession 0270533.

Romagosa, M., M. Baumgartner, I. Cascão, M. O. Lammers, T. A. Marques, R. S. Santos, and M. A. Silva (2020). Baleen whale acoustic presence and behaviour at a Mid-Atlantic migratory habitat, the Azores Archipelago, *Sci. Rep.* **10,** 4766, doi: 10.1038/s41598-020-61849-8.

Ryan, W. B. F., S. M. Carbotte, J. O. Coplan, S. O'Hazra, A. Melkonian, R. Arko, R. A. Weissel, V. Ferrini, A. Goodwillie, F. Nitsche, *et al.* (2009). Global multi-resolution topography synthesis, *Geochem. Geophys. Geosys.* **10,** Q03014, doi: 10.1029/2008GC002332.

Shearer, P. M. (2019). *Introduction to Seismology*, Cambridge University Press, Cambridge, UK.

Stein, S., and M. Wysession (2009). *An Introduction to Seismology, Earthquakes, and Earth Structure*, John Wiley and Sons, Oxford, UK.

Talling, P. J. (2014). On the triggers, resulting flow types and frequencies of subaqueous sediment density flows in different settings, *Mar. Geol.* **352,** 155–182, doi: 10.1016/j.margeo.2014.02.006.

Talling, P. J., M. L. Baker, E. L. Pope, S. C. Ruffell, R. S. Jacinto, M. S. Heijnen, S. Hage, S. M. Simmons, M. Hasenhündl, C. J. Heerema, *et al.* (2022). Longest sediment flows yet measured show how major rivers connect efficiently to deep sea, *Nat. Commun.* **13,** no. 1, 4193, doi: 10.1038/s41467-022-31689-3.

Talling, P. J., M. J. B. Cartigny, E. Pope, M. L. Baker, M. A. Clare, S. Hage, M. S. Heijnen, D. R. Parsons, S. Simmons, *et al.* (2023). Detailed monitoring reveals the nature of submarine turbidity currents, *Nat. Rev. Earth Environ.* **4,** 642–658, doi: 10.1038/s43017-023-00458-1.

Talling, P. J., M. Clare, M. Urlaub, E. Pope, J. E. Hunt, and S. F. L. Watt (2014). Large submarine landslides on continental slopes: Geohazards and role in methane release and climate change, *Oceanography* **27,** 32–45, doi: 10.5670/oceanog.2014.38.

Talling, P. J., C. K. Paull, and D. J. W. Piper (2013). How are subaqueous sediment density flows triggered, what is their internal structure and how does it evolve? Direct observations from monitoring of active flows, *Earth Sci. Rev.* **125,** 244–287, doi: 10.1016/j.earscirev.2013.07.005.

Tepp, G., and R. P. Dziak (2021). The seismo-acoustics of submarine volcanic eruptions, *J. Geophys. Res.* **126,** e2020JB020912, doi: 10.1029/2020JB020912.

The Economist (2024). Damage to undersea cables is disrupting internet access across Africa, available at https://www.economist.com/middle-east-and-africa/2024/03/21/damage-to-undersea-cables-is-disrupting-internet-access-across-africa (last accessed July 2024).

Urlaub, M., and H. Villinger (2019). *Combining in Situ Monitoring Using Seabed Instruments and Numerical Modelling to Assess the Transient Stability of Underwater Slopes*, Vol. 477, Geological Society, London, United Kingdom, Special Publications, 511–521, doi: 10.1144/SP477.8.

Vardy, M. E., J. S. L'Heureux, M. Vanneste, O. Longva, A. Steiner, C. F. Forsberg, H. Haflidason, and J. Brendryen (2012). Multidisciplinary investigation of a shallow near-shore landslide, Finneidfjord, Norway, *Near Surf. Geophys.* **10,** no. 4, 267–277, doi: 10.3997/1873-2012022.

Wessel, P., J. F. Luis, L. Uieda, R. Scharroo, F. Wobbe, W. H. F. Smith, and D. Tian (2019). The generic mapping Tools version 6, *Geochem. Geophys. Geosys.* **20,** no. 11, 5556–5564, doi: 10.1029/2019GC008515.

Wright, I. C., W. W. Chadwick, C. E. J. de Ronde, D. Reymond, O. Hyvernaud, H.-H. Gennerich, P. Stoffers, K. Mackay, M. A. Dunkin, and S. C. Bannister (2008). Collapse and reconstruction of Monowai submarine volcano, Kermadec arc, 1998-2004, *J. Geophys. Res.* **113,** no. B8, doi: 10.1029/2007JB005138.

Manuscript received 8 November 2024
Published online 26 March 2025